วิศวกรรมสาร ม.ข. ปีที่ 30 ฉบับที่ 4 (391-406) ตุลาคม-ธันวาคม 2546
KKU Engineering Journal Vol. 30 No. 4 (391-406) October-December 2003

แบบจำลองโครงข้อแข็งอันดับสูงสำหรับการวิเคราะห์แบบไม่เชิงเส้นของคาน ค.ส.ล. ที่เสริมกำลังการดัดด้วยการติดแผ่นเสริมกำลังจากภายนอก

สุชาติ ลิ่มกตัญญู และ เอกรัฐ สมัครัฐกิจ
ภาควิชาวิศวกรรมโยธา คณะวิศวกรรมศาสตร์มหาวิทยาลัยสงขลานครินทร์ อ.หาดใหญ่ จ.สงขลา
E-mail: lsuchart@ratree.psu.ac.th และ Sagarat@ratree.psu.ac.th

บทคัดย่อ

อาคารและโครงสร้างพื้นฐาน ในลักษณะโครงสร้างคอนกรีตเสริมเหล็ก (ค.ส.ล.) จำนวนมากในปัจจุบันมีความไม่สอดคล้องกับข้อกำหนดในการออกแบบในปัจจุบัน ทั้งนี้อาจเนื่องจากการเสื่อมสภาพที่มีสาเหตุจากการทำลายของสิ่งแวดล้อมเช่น การเสื่อมสภาพเนื่องจากคลอไรด์หรือการออกแบบบนพื้นฐานเก่า ซึ่งไม่เพียงพอกับเกณฑ์ในปัจจุบัน การเสริมกำลังจึงมีความสำคัญทั้งในการเพิ่มระดับความปลอดภัยของโครงสร้างเพื่อให้สอดคล้องข้อกำหนดในปัจจุบัน และประหยัดค่าใช้จ่ายในการก่อสร้างโครงสร้างใหม่ วิธีการในปัจจุบันสำหรับการเพิ่มกำลังการดัดของคาน ค.ส.ล. คือ การใช้แผ่น FRP ทากาวยึดติดด้านที่รับแรงดึงของคาน อย่างไรก็ตามรูปแบบการวิบัติของคาน ค.ส.ล. ที่เสริมกำลังการดัดด้วยวิธีนี้โดยส่วนใหญ่จะเนื่องจากการหลุดหล่อนของแผ่นเสริมที่ระดับของแรงกระทำซึ่งต่ำกว่าค่าที่คำนวนทางทฤษฎี ดังนั้น แบบจำลองการวิเคราะห์ที่รวมผลการวิบัติที่เกิดจากการหลุดหล่อนของแผ่นเสริม จึงจำเป็นต่อการพัฒนาโปรแกรมที่น่าเชื่อถือทางคณิตศาสตร์ ในบทความจะนำเสนอชิ้นส่วนโครงสร้างอันดับสูงบนพื้นฐานการเคลื่อนที่ที่พิจารณาผลการยึดรั้งของคอนกรีต การเลื่อนตัวระหว่างผิวคานกับแผ่นเสริมกำลังถูกแยกคำนึงในส่วนของคาน และแผ่นเสริมกำลัง แบบจำลองที่นำเสนอถูกตรวจสอบความถูกต้อง ด้วยการศึกษาเปรียบเทียบกับผลจากการทดลอง

Higher-Order Frame Model for Nonlinear Analysis of RC Beams Strengthened in Flexure with Externally Bonded Plates

Suchart Limkatanyu and Agarat Samakrattakit
Department of Civil Engineering, Faculty of Engineering, Prince of Songkla University, Hadyai, Songkhla, Thailand, 90112
E-mail: lsuchart@ratree.psu.ac.th and sagarat@ratree.psu.ac.th

Abstract

Many existing reinforced concrete (RC) structures very often do not satisfy building codes used nowadays to design both buildings and infrastructures because they have either deteriorated due to environmental attacks (e.g. chloride induced deterioration) or because they were originally designed according to old and inadequate criteria. Retrofitting and/or strengthening are necessary in order to increase the safety level of the structure according to the building codes today in use and to save the cost for replacing the existing structure. A recent methodology to enhance the flexural strength of RC beams uses FRP plates or sheets glued to the tension side of the beam. A commonly observed failure mode for the beams strengthened in flexure with externally bonded plate is the one associated with debonding of the strengthening plates at lower loading levels than the theoretical values. Consequently, the inclusion of the plate-debonding failure into the analytical model is necessary in developing the reliable numerical tool. This paper presents a higher-order displacement-based frame element with covercrete-interface. The covercrete-interface slip between the beam and the plate is taken in account through separating displacement fields in the beam and in the strengthening plate. The proposed model is employed to confirm and investigate premature failure modes observed in experimental tests.

keywords: frame model, displacement-based formulation, nonlinear analysis, FRP composites materials, RC beams strengthening, debonding failure.

Introduction

Several techniques have been used to strengthen or to rehabilitate the existing reinforce concrete (RC) or prestressed concrete (PC) structures (Emmons, Vaysburd, and Thomas, 1998). Enlarging structural sections usually result in a monolithic element of increased dimension. The common use of sectional enlargement technique is in bridge deck rehabilitation and strengthening, where it has the advantage of being comparative simple to implement and can be both economic and effective. There, however, exists a high potential of concrete deterioration induced by the incompatibility of old and new concrete, hence resulting in corrosion of the embedded steel reinforcement. In addition, it can change significantly the structural dimensions with a corresponding loss of clearance. External prestressing techniques are an alternative method for

strengthening and have been widely used to remedy excessive deflections and to enhance the load-carrying capacity (Klaiber, Dunker, and Sanders, 1987; Saadatmanesh, Albrecht, and Ayyub, 1989). Nevertheless, the provision of sufficient anchorage for the post-tensioning strands, the durability of the exposed strands, the lateral stability of the beams during post-tensioning, and the preservation of existing clearance dimensions are problems possibly putting the limitations of this strengthening technique.

Epoxy-bonded steel plate has been used efficiently throughout the world to enhance the load-carrying capacity of existing reinforced concrete structures (Dussek, 1980; MacDonald and Calder, 1982; Swamy, Jones, and Bloxham, 1987). This strengthening technique has been found by civil engineers to be economical and effective to implement. The concept of this strengthening method is somewhat simple. Steel plates are bonded to the tension region, thus increasing the strength and stiffness of the beam. The advantages of this structural system include the ease of application and elimination of special anchorages required in the post-tensioning method. Strengthening process can be performed while the structures are still functioning and it does not change the structural dimensions. However, a major hamper of this technique is the risk of corrosion at the epoxy-steel interface that contrarily affects the bond-interface strength.

To overcome the corrosion problem, the steel plate is replaced with corrosion-proof Fiber Reinforced Polymer (FRP) plate. Since the early 1990s, extensive researches have been conducted on tests of FRP strengthened RC beams and have shown that the substantial improvement can be gained in structural performance under both service and ultimate loading stages. Concurrently, the new brittle failure mechanism of strengthened beams has been found, mostly due to premature plate debonding (Oehlers, and Moran, 1989; Saadatmanesh, and Ehsani, 1991; Arduini, Tommaso, and Nanni, 1997; Arduini, and Nanni, 1997; Zarnic, Gostic, Bosiljkov, and Bokan-Bosiljkov, 1999). In order to realistically predict the beam loading capacity and the failure mode associated with plate debonding, it is crucial to use analytical model capable of describing the bond-force evolution along the covercrete-interface between the beam and the strengthening plate.

Several analytical models have been proposed in the research community for the calculation of the stresses developing at the covercrete-interface interface in the uncracked RC beams (Roberts, 1989; Täljsten, 1997; Malek, Saadatmanesh, and Ehsani, 1998; Rabinovich, and Frostig, 2000). However, these analytical models are valid only for elastic analysis and uncracked sections, which are far from reality during ultimate loading stages.

Recently, significant advances in modeling the nonlinear response of RC members were achieved in recent years, lead by the development of beam models that rely on the fiber section model. Fiber section models naturally account for the coupling between axial and bending effects (Spacone, Filippou, and Taucer, 1996) and can be combined with any beam element model including displacement-based and force-based models. Fiber section models are typically based on the assumption that plane sections remain plane, and thus neglect bond-slip effects. The bond-slip

effects can be added in different ways: (*a*) by using nonlinear springs at the element ends (Rubiano-Benavides, 1998). This approach, however, is not readily extended to the study of RC beams strengthened with externally bonded thin plates; (*b*) by modifying the fiber section model to relax the compatibility between concrete and steel strains (Monti, and Spacone, 2000); (*c*) by modeling the steel rebars and the concrete beam with different degrees of freedom (Limkatanyu, and Spacone, 2002).

The numerical model used in this paper is the higher-order modification of the displacement-based RC frame element with bond-interface (Limkatanyu, and Spacone, 2002). The element is very easy to formulate and to implement. The model can properly describe the shear stress distributions that arise during loading of the RC beam up to failure. This model introduces an elasto-fragile bond law for the covercrete-interface behavior and takes into account the nonlinear behavior of the materials including the tension stiffening of concrete in tensile areas. Available experimental data are used to validate the proposed modeling technique and to investigate different failure mechanisms.

Higher-Order Displacement-Based Fiber Frame Model with Covercrete-Interface

The displacement-based RC frame model with covercrete-interface used in the present study is shown in Figure 1. The element formulation is presented hereafter. In this model, the covercrete springs are laid along the interface between the concrete beam and the externally bonded plate. Plates bonded to the sides of the beams for shear strengthening are not taken into account, since this study emphasizes primarily on the flexural behavior. The strengthening plate is assumed thin, thus it only carry axial load, and has no shear or flexural stiffness.

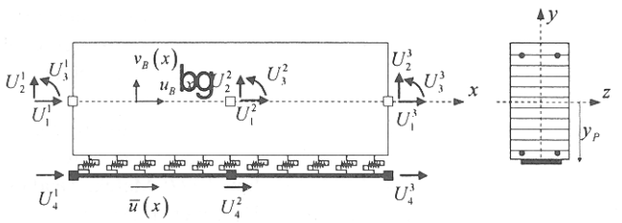

$$\mathbf{u}(x) = \{u_B(x) \quad v_B(x) \mid \bar{u}(x)\}^T$$

$$\mathbf{U} = \{U_1^1 \quad U_2^1 \quad U_3^1 \quad U_4^1 \quad \text{M} \quad U_1^2 \quad U_2^2 \quad U_3^2 \quad U_4^2 \quad \text{M} \quad U_1^3 \quad U_2^3 \quad U_3^3 \quad U_4^3\}^T$$

Figure 1 Node and Element displacements for RC Frame Model with Slip in the Strengthening Plate

The RC frame element with covercrete-interface consists of two components: beam-column element representing the RC beam and bar element representing the strengthening plate. These two ingredients are mutually interacted

through continuous tangential springs along the covercrete-interface. The nodal degrees of freedoms of the RC beam and of the strengthening plate are different in order to create the tangential slip field along the covercrete-interface. The element nodal displacements and element displacement fields are indicated in Figure 1 and are grouped in vectors **U** and $\mathbf{u}(x)$, respectively. The internal node is introduced in order to enhance the element accuracy over the 2-node displacement-based element [19]. The fiber-section discretization is used to derive the sectional response of the RC beam. The section-deformation fields are written in the vector format as $\mathbf{d}(x)=\left[\varepsilon_B(x)\ \ \kappa_B(x)\ \ \text{м}\,\bar{\varepsilon}(x)\right]^T$, where $\varepsilon_B(x)$ represents the beam-section axial strain, $\kappa_B(x)$ represents the beam-section curvature, and $\bar{\varepsilon}(x)$ represents the plate axial strain. The kinematics of beam deformations is based on the Euler-Bernoulli beam hypothesis, thus implying that plane sections are assumed to remain plane and are normal to the beam longitudinal axis. Based on the small-deformation theory, the beam-section deformations are related to the beam displacements through the compatibility equations:

$$\begin{aligned}\varepsilon_B(x)&=\frac{du_B(x)}{dx}\\ \kappa_B(x)&=\frac{d^2v_B(x)}{dx^2}\\ \bar{\varepsilon}(x)&=\frac{d\bar{u}(x)}{dx}\end{aligned}\qquad(1)$$

where $u_B(x)$ is the beam axial displacement, $v_B(x)$ is the beam transverse displacement, and $\bar{\varepsilon}(x)$ is the plate axial displacement. The sectional forces conjugate of $\mathbf{d}(x)$ are $\mathbf{D}(x)=\left\lfloor N_B(x)\ \ M_B(x)\ \ \text{м}\ \ \bar{N}(x)\right\rfloor^T$, where $N_B(x)$ is the beam-section axial force, $M_B(x)$ $M_B(x)$ is the beam-section moment, and $\bar{N}(x)$ is the plate axial force. The slip field $u_b(x)$ along the covercrete-interface can be described as:

$$u_b(x)=\bar{u}(x)-u_B(x)+y_P\left[\frac{dv_B(x)}{dx}\right]\qquad(2)$$

where $dv_B(x)/dx$ represents the beam section rotation and y_P represents the plate distance from the beam reference axis as shown in Figure 1.

The element displacements $\mathbf{u}(x)$ are related to the element nodal displacements **U** through the displacement shape functions $\mathbf{N}_u(x)$ as follows:

$$\mathbf{u}(x) = \begin{Bmatrix} \mathbf{u}_B(x) \\ \overline{u}(x) \end{Bmatrix} = \begin{Bmatrix} \mathbf{N}_{uB}(x) \\ \mathbf{N}_{\overline{u}}(x) \end{Bmatrix} \mathbf{U} = \mathbf{N}_u(x)\mathbf{U} \tag{3}$$

where $\mathbf{N}_{uB}(x)$ is the matrix containing the shape functions of a three-node beam element. They are polynomial functions that define a quadratic axial displacement field and a 5th-order vertical displacement field. $\mathbf{N}_{\overline{u}}(x)$ contains the polynomial functions of the strengthening plate axial displacement field, which are quadratic in the present formulation.

The compatibility conditions of beam and of covercrete-interface are satisfied in the point-wise sense. The section and covercrete-interface deformations are directly related to the nodal displacements $\mathbf{U}$ through the following equations:

$$\mathbf{d}(x) = \mathbf{B}_u(x)\mathbf{U}; \quad u_b(x) = \mathbf{B}_b(x)\mathbf{U} \tag{4}$$

where $\mathbf{B}_u(x) = \partial\, \mathbf{N}_u(x)$, $\mathbf{B}_b(x) = \partial_b \mathbf{N}_u(x)$ when ∂ and ∂_b are linear differential operators and are defined as:

$$\partial = \begin{bmatrix} \frac{d}{dx} & 0 & 0 \\ 0 & \frac{d^2}{dx^2} & 0 \\ 0 & 0 & \frac{d}{dx} \end{bmatrix}; \quad \partial_b = \begin{Bmatrix} -1 & y_p \frac{d}{dx} & 1 \end{Bmatrix} \tag{5}$$

Element equilibrium, however, is enforced in the integral sense. Application of the principle of virtual displacements, substitution of Eq.(4) and subsequent elimination of the virtual nodal displacements $\delta\mathbf{U}$, yield the following weak form of equilibrium statement:

$$\int_L \mathbf{B}_u^T(x)\,\mathbf{D}(x)\,dx + \int_L \mathbf{B}_b^T(x)\,D_b(x)\,dx = \mathbf{P} \tag{6}$$

where $\mathbf{P}$ is the applied nodal forces conjugate of nodal displacements $\mathbf{U}$; and $D_b(x)$ is the bond force along the covercrete-interface between the beam and the plate.

In order to obtain the incremental form of equilibrium, the total internal forces are expressed as the sum of the initial section forces $\mathbf{D}^0(x)$ and $D_b^0(x)$ plus the force increments $\Delta\mathbf{D}(x) = \mathbf{k}(x)\Delta\mathbf{d}(x)$ and $\Delta D_b(x) = k_b(x)\Delta u_b(x)$. $\mathbf{k}(x)$ is the beam section stiffness matrix and $k_b(x)$ is the covercrete-interface stiffness. Then:

$$\begin{aligned} &\int_L \mathbf{B}_u^T(x)\left[\mathbf{D}^0(x) + \mathbf{k}(x)\,\mathbf{B}_u^T(x)\Delta\mathbf{U}\right]dx + \\ &\int_L \mathbf{B}_b^T(x)\left[D_b^0(x) + k_b(x)\,\mathbf{B}_b(x)\Delta\mathbf{U}\right]dx = \mathbf{P} \end{aligned} \tag{7}$$

or, upon simplification:

$$\mathbf{K}\,\Delta\mathbf{U} = \mathbf{P} - \mathbf{Q}^0 \tag{8}$$

where the element stiffness matrix $\mathbf{K}$ can be described as:

$$\mathbf{K} = \mathbf{K}_B + \mathbf{K}_b \tag{9}$$

where $\mathbf{K}_B$ and $\mathbf{K}_b$ are the contributions of the beam and of the covercrete-interface to the element stiffness matrix, respectively.

$$\mathbf{K}_B = \int_L \mathbf{B}_u^T(x)\,\mathbf{k}_B\,\mathbf{B}_u(x)\,dx \tag{10}$$

$$\mathbf{K}_b = \int_L \mathbf{B}_b^T(x)\,k_b\,\mathbf{B}_b(x)\,dx \tag{11}$$

$\mathbf{Q}^0$ is the vector containing the element resisting forces at the initial iterative step:

$$\mathbf{Q}^0 = \mathbf{Q}_B^0 + \mathbf{Q}_b^0 \tag{12}$$

where $\mathbf{Q}_B^0$ and $\mathbf{Q}_b^0$ are the beam and covercrete-interface contributions to the element resisting forces, respectively and can be expressed as:

$$\mathbf{Q}_B^0 = \int_L \mathbf{B}_u^T(x)\,\mathbf{D}_B^0(x)\,dx \tag{13}$$

$$\mathbf{Q}_b^0 = \int_L \mathbf{B}_b^T(x)\,D_b^0(x)\,dx \tag{14}$$

It is noteworthy to point out that the right-hand side of Eq.(8) is the force residual corresponding to the weak statement of the element equilibrium and vanishes once the equilibrium configuration is gained.

In the present work, the fiber section model is used to compute the response of the RC beam section. Well-established uniaxial cyclic constitutive laws for concrete, steel and covercrete-interface complete the element formulation. The loading envelopes of these laws are schematically shown in Figure 2. The Kent and Park model (Kent, D. C., and Park, 1964-1990) is used for the concrete, with the addition of the tension response, which is assumed linear elastic up to the cracking stress f_t', with rapid linear stress degradation for increasing tensile strains. The Menegotto and Pinto model (Menegotto, and Pinto, (Menegotto, and Pinto, 1973) is used for the steel rebars. For the covercrete-interface between the beam and the strengthening plate, a curve linear up to the point of bond failure is used. The above element formulation can be implemented in any general-purpose nonlinear finite element code. In the present study, the element is implemented in program FEAP, documented in Taylor (Taylor, 2000).

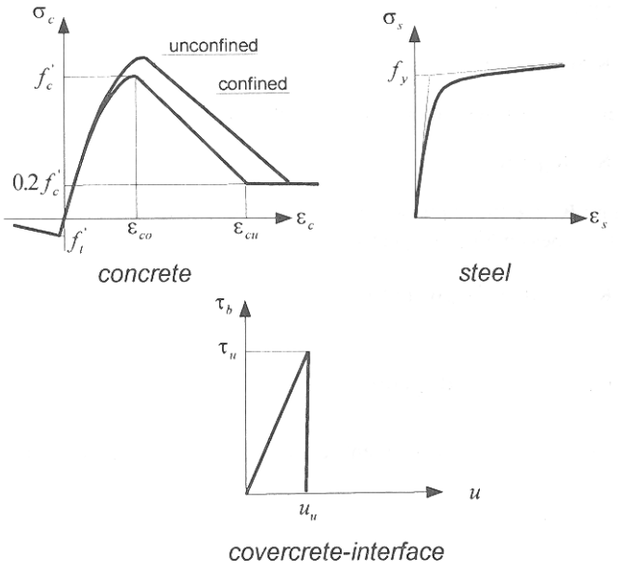

Figure 2 Material Constitutive Models

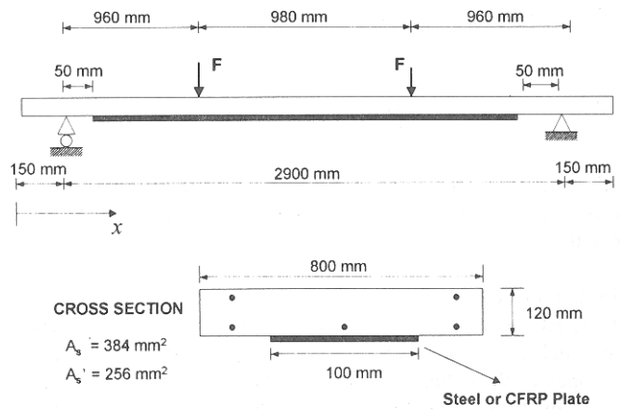

Figure 3 Test Setup for Shallow RC Beams with Steel or CFRP Plates

Zarnic et al. RC Slabs Strengthened by Externally Bonded CFRP and Steel Plates

Zarnic et al. (Zarnic, Gostic, Bosiljkov, and Bokan-Bosiljkov, 1999) performed an experimental test on a series of RC beams strengthened in flexure with externally bonded CFRP and steel plates. During the tests, several failure mechanisms were observed. Of particular interest to the present work is the test of

shallow beams strengthened in flexure with externally bonded steel and CFRP plates. The specimen dimension and the test setup are shown in Figure 3. The strengthening plates are 100 m- wide and 4 and 1.2 mm thick for steel and CFRP, respectively. The displacement-control technique was used for both experimental and numerical investigations. In the numerical model, only half of the specimen is considered due to the symmetry of the loading and of the specimen. The specimen is discretized into 24 elements as shown in Figure 4 to obtain a smooth bond-stress distribution along the covercrete-interface. 7 elements, however, are sufficient to gain the same overall result.

Following Zarnic et al. (Zarnic, Gostic, Bosiljkov, and Bokan-Bosiljkov, 1999), the following material parameters are used in the numerical analysis: for concrete $f_c' = 25$ MPa and $f_t' = 1$ MPa; for steel $f_y = 460$ MPa and $E_s = 210,000$ MPa; for steel plate $f_y = 360$ MPa and $E_{sp} = 210,000$ MPa; for CFRP plate $f_u = 2,400$ MPa and $E_{CFRP} = 150$ GPa; for covercrete-interface $f_u = 3.0$ MPa and $E_b = 2,384$ MPa/mm. For this study, the covercrete-interface law is linear elastic up to the point of failure as shown Figure 2 and the material parameters are obtained the calibration with the interface model proposed by Chen and Teng (Chen, and Teng, 2001).

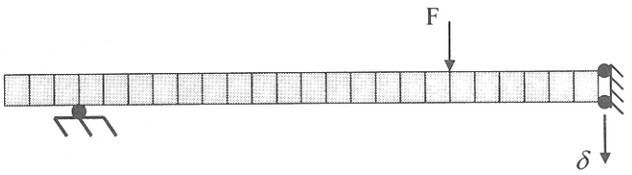

Figure 4 Finite Element Mesh

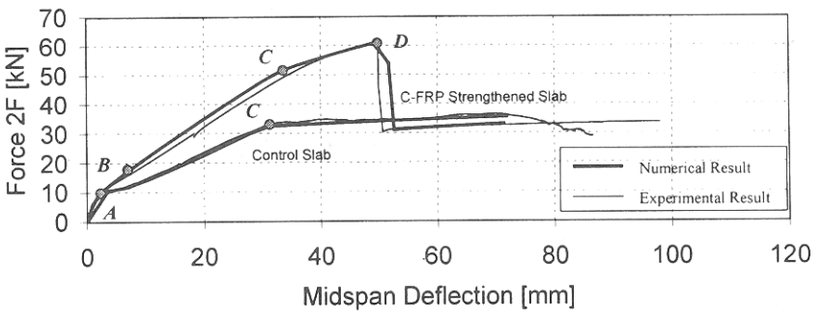

Figure 5 Experimental and Numerical Responses of C-FRP Strengthened and Control Slabs

CFRP Strengthened RC Slab

In the case of CFRP strengthened RC slab, Figure 5 shows the correlation study between experimental and numerical results. Clearly, there are good agreements between experimental and numerical results in terms of both stiffness and strength. Four distinct loading stages are indicated on the numerical response curves. Point *A* indicates the loading stage at which the middle third (constant moment region) of the beam cracks, followed by a decrease in the beam stiffness. Point *B* represents the loading stage at which cracking propagates toward the beam end but the bottom steel reinforcement is still elastic. The steep change in stiffness between Points *A* and *B* is due to the initial rapid propagation of the cracking toward the beam end, which advances with the inverse of the applied force F. Point *C* represents the loading stage at which the bottom steel reinforcement yields, hence resulting in another significant drop in the response stiffness. Finally, Point *D* represents the loading stage at which the CFRP plate debonds. At this point, both experimental test and numerical response show a large drop in beam strength due to the loss of the plate contribution. The residual strength is that of the control (nonstrengthened) slab. It is also worthwhile to point out that the force-displacement response of the control (nonstrengthened) slab is much more ductile than that of the CFRP strengthened slab.

The tensile force distributions in the CFRP plate along the beam for Points *B*, *C*, and *D* in Figure 5 are shown in Figure 6. The tensile force in the plate has a fairly smooth distribution. It has zero value at the plate end (200 mm from the beam end), then increases up to the point of the applied load (1,100 mm from the beam end), and finally, remains constant in the constant moment region. Two distinct points on the force distributions mark a clear change in the force slope between the plate end and the point of load application. The first point, labeled as b in Figure 6, distinguishes cracked and uncracked sections. Cracking never reaches the section at the plate end, because it is preceded by the plate-debonding failure. The second point, labeled as d in Figure 6, corresponds to the section where the bottom steel reinforcement yields. The bottom steel reinforcement has yielded to the right of Point d, and is still elastic to the left. Point d moves to the left from distribution *C* to *D* in Figure 6, resulting from yield penetration as the applied load increases.

Figure 7 shows the corresponding bond force distributions along the covercrete-interface. It is important to note that the bond force is proportional to the first derivative of the force in the plate. Furthermore, the slip field along the concrete-interface contains the first derivative of the transverse displacement Eq.(2); thus its approximation is less accurate than that of the transverse displacement field. The bond stress has zero value in the central third of the beam, where the moment is constant. Starting from the point of applied load and moving to the left toward the beam end, the bond values gradually decrease. There are two points of discontinuities marked on the bond-stress distributions as shown in Figure 7. The first point, labeled as a in Figure 7 is located at the end of the plate and the second point, labeled as c in Figure 7 is located near the applied load. The bond discontinuity at the free end is a well-known phenomenon, discussed in detail by

Täljsten (Täljsten, 1997). The jump in bond stress at this point is due to the sudden change in cross section. The bond discontinuity at the point of load application is due to the sudden drop in tensile force in the plate outside the region of constant moment. This point is the beginning of the anchorage zone for the plate. The local peak at the point of load application becomes sharper as larger loads are applied. For the bond force distribution that corresponds to loading point *B*, bond increases sharply near the point of load application, and then decreases until point b, which separates cracked and uncracked regions. Bond drops to almost zero at point b. At loading point *B* the bottom steel rebars are still linear elastic. At loading point *C* the bottom steel rebars start yielding (in the middle third of the beam). After the peak point (labeled c), bond drops drastically and remains constant over a cracked region where the steel rebars are still elastic. A similar bond stress distribution is observed at loading point *D*, but the bond-stress values are larger and there is a short plateau of almost constant bond after point c. This plateau, which roughly corresponds to the region where the bottom steel has yielded, ends at point d, beyond which the bottom steel is still elastic. According to the bond distribution at load level *D*, the failure of this specimen is caused by debonding of the plate at the loading point. This failure mode was observed during the test.

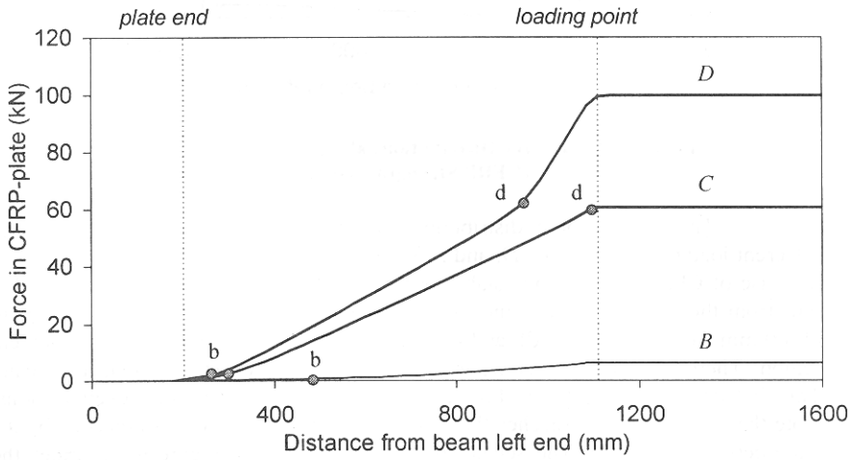

Figure 6 Tension Force Distributions in C-FRP Plate along Beam

Steel Strengthened RC Slab

In the case of steel strengthened RC slab, the correlation study between experimental and numerical results is presented in Figure 8. Obviously, the proposed numerical model can predict well not only the strengths but also the stiffness of the specimens. There are five distinct loading points marked on the numerical response curves in Figure 8. Point *A* marks the onset of concrete cracking in the constant moment region of the beam and is followed by a decrease in the beam stiffness. Point *B* represents a generic loading stage at which cracking propagates toward the beam end but the bottom steel reinforcement and the strengthening steel plate are

still in the elastic range. Point *C* indicates the point where the strengthening plate yields. Point *D* represents the loading stage at which the bottom steel reinforcement yields. As expected, the strengthening steel plate yields before the bottom steel reinforcement yields. After the bottom steel reinforcement yields, the beam stiffness is very small and mainly due to the hardening properties of steel reinforcements. Point *E* represents the loading stage at which the steel plate debonds.

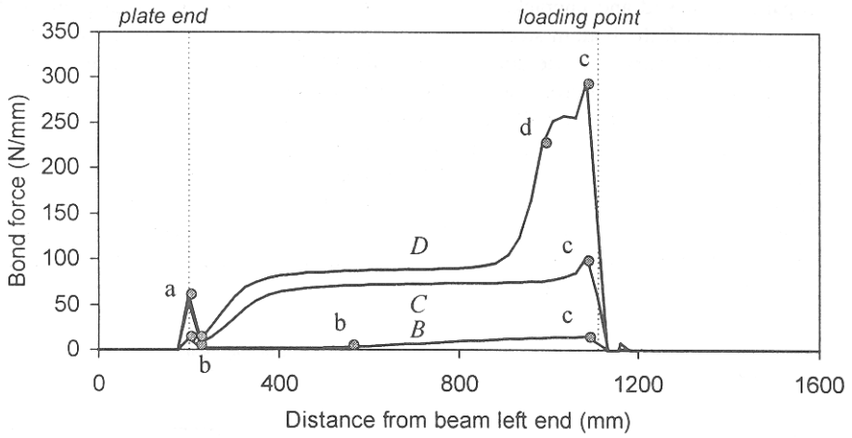

Figure 7 Bond Force Distributions along Covercrete-Interface (CFRP Strengthened Slab)

The tensile force distributions in the steel plate along the beam for different loading stages; *B*, *C*, *D*, and *E* in Figure 8 are shown in Figure 9. Similar to the case of CFRP strengthened slab, the force in plate is zero at the plate end (200 mm from the beam end), then increases up to the maximum value at the load point (1100 mm from the beam end), and finally, remains constant in the constant moment region. There are three points separating the beam-section stages along the beam. The first point, labeled as a in Figure 9, separates cracked and uncracked sections. Note that cracking never reaches the plate-end section, because it is preceded by the plate-debonding failure. The second point, labeled as b in Figure 9, separates the region where the steel plate has already yielded (to the right of b) from the region where the steel plate is yet to yield (to the left of b). The third point, labeled as c in Figure 9, separates the region where the bottom steel reinforcement has already yielded (to the right of c) from the region where the bottom steel reinforcement is yet to yield (to the left of c). Points b and c move to the left from distributions *C* to *E* in Figure 9, resulting from the yielding penetration of the steel reinforcement as the applied load increases.

The corresponding bond force distributions along the covercrete-interface are shown in Figure 10. The bond force is zero near the loading point, up to the point b, which marks the separation between yielded and non-yielded steel plate. Directly to the left of point b, the bond force precipitously increases from zero to an

almost constant value until point a separating the cracked and uncracked sections. As the applied load increases, the plate yield front (point b) propagates to the left and, as a result, the bond discontinuity and the intermediate plateau values increase as well. This bond force increase is resulted from the shortening of the plate anchorage length spanning from point b to the plate end. As the anchorage length decreases, the bond forces must increase in order to maintain equilibrium. At load level *D*, the covercrete-interface strength is reached in several sections between the plate end and the loading point and is not as locally as in the case of CFRP strengthened slab (Figure 7). This can possibly explain why the failure mechanism of this specimen was not clearly detected in the experimental investigation.

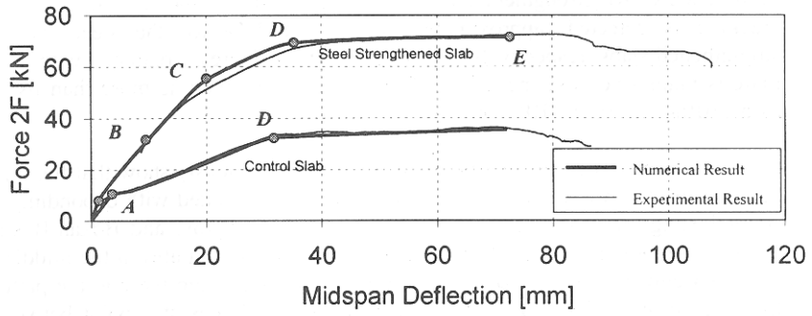

Figure 8 Experimental and Numerical Responses of Steel Strengthened and Control Slabs

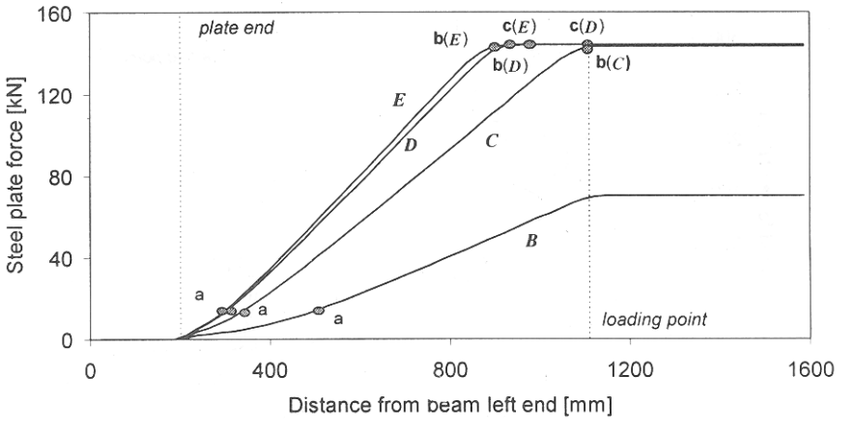

Figure 9 Tension Force Distributions in Steel Plate along Beam

Observations of Numerical Investigation

A few important observations can be drawn from the experimental and numerical results plotted in Figure 5 and Figure 8. First, due to the externally bonded plate, the loading capacity of the specimens is substantially enhanced. In the case of the CFRP strengthened slab, the increase is more or less 73% while in the case of the steel strengthened slab, the increase is approximately 98%. Notwithstanding, because of the plate debonding, the substantial increase in loading capacity is followed by the loss of overall ductility of the strengthened specimens. It is important to note that the control slab is under-reinforced. The steel strengthened slab shows a ratio of failure-to-yield deflection that is sensibly larger than the same ratio of the CFRP strengthened slab. Finally, a significant increase in stiffness after cracking is detected: approximately 145% and 72% for the steel and CFRP strengthened slabs, respectively. The larger stiffness increase obtained with the steel plate is mainly because the axial stiffness of the steel plate is more than twice the axial stiffness of the CFRP plate.

Both experimental and numerical results obviously show that the ultimate failure condition for all strengthened specimens is associated with debonding of the strengthening plate. Zarnic et al. (Zarnic, Gostic, Bosiljkov, and Bokan-Bosiljkov, 1999), observed that the CFRP plate detachment always initiates in the middle third of the specimen under the loading point and propagates from there to the plate end. In the case of steel strengthened slab, detachment initiates at a point between the plate end and the loading point. Conclusively, the overall tendencies of numerical simulations performed in the present study are supported by experimental observations.

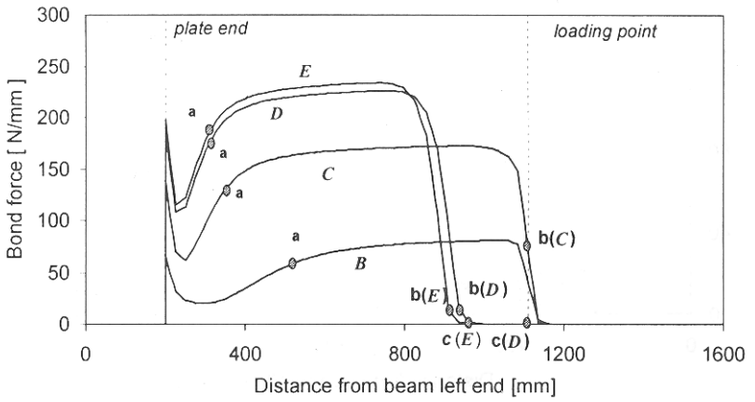

Figure 10 Bond Force Distributions along Covercrete-Interface (Steel Strengthened Slab)

It is worthwhile to point out that, although debonding always causes a sudden failure, debonding in the steel strengthened slabs occurs long after the strengthening plate has yield and the maximum loading capacity has been reached,

thus providing good ductility in the force-displacement curve (Figure 8). On the other hand, in the CFRP strengthened plate, the plate debonds when the slab response is still hardening, before the plate reaches its ultimate strength. Consequently, the strengthening efficiency is not totally exploited because of a premature failure. As a matter of fact, the axial strain in CFRP plate at debonding failure is only 5.5%. This value is more or less half the strain expected at the load level that would cause concrete crushing (within the assumption that the covercrete-interface strength is infinite).

conclusions

This study points out the importance of including covercrete-interface into the numerical model for nonlinear analysis of RC shallow beams strengthened in flexure with either thin steel or thin CFRP plates. The numerical simulations are relied on a simple but accurate displacement-based frame element with covercrete-interface between the RC beam and the strengthening plate. Numerical simulations of a series of experimental tests by Zarnic et al. (Zarnic, Gostic, Bosiljkov, and Bokan-Bosiljkov, 1999), indicate that the covercrete-interface forces and the covercrete-interface failure between the RC beam and the strengthening plates are the crucial issues in strengthening of shallow RC beams and must considered to evaluate the effective stiffness and loading capacity of the strengthened members. Especially, implementation of an elastic-brittle covercrete-interface law yields thorough information on the evolution of the failure mechanism under increasing applied loads.

References

Arduini, M., Di Tommaso, A., and Nanni, A. 1997. "Brittle Failure in FRP Plate and Sheet Bonded Beams." **ACI Structural Journal**. 94, 4: 363-369.

Arduini, M. and Nanni, A. 1997. "Behavior of Pre-Cracked RC Beams Strengthened with Carbon FRP Sheets." **ASCE Journal of Composites for Construction**. 1, 2: 63-70.

Chen, J.F. and Teng, J.G. 2001 "Anchorage Strength Models for FRP and Steel Plates Attached to Concrete." **ASCE Journal of Structural Engineering**. 127, 7: 784-791.

Dussek, I.J. 1980. "Strengthening of Bridge Beams and Similar Structures by means of Epoxy-Resin-Bonded External Reinforcement." **Transportation Research Board**. Report No. 785

Emmons, P.H., Vaysburd, A.M., and Thomas, J. 1998. "Strengthening Concrete Structures: Part I." **ACI Concrete International, March**. : 53-58.

Kent, D. C., and Park, R. 1971. "Flexural Members with Confined Concrete." **ASCE Journal of the Structural Division**. 97,7: 1964-1990.

Klaiber, F.W., Dunker, K.F., and Sanders, W.W., Jr. 1987. "Methods of Strengthening Existing Highway Bridges." **National Cooperative Highway Research Program**. Report No. 293.

Limkatanyu, S, and Spacone, E. 2002. "R/C Frame Element with Bond Interfaces. Part I: Displacement-Based, Force-Based and Mixed Formulations." **ASCE Journal of Structural Engineering**. 128,3: 346-355.

MacDonald, M.D. and Calder, A.J.J. 1982. "Bonded Steel Plating for Strengthening Concrete Structures." **International Journal of Adhesion and Adhesives** 2, 2: 119-127.

Malek, A.M., Saadatmanesh, H., and Ehsani, M.R. 1998. " Prediction of Failure Load of RC Beams Strengthened with FRP plate due to Stress Concentration at the Plate End." **ACI Structural Journal**. 95,1: 142-152.

Menegotto, M., and Pinto, P. E. 1973. "Method of Analysis for Cyclically Loaded Reinforced Concrete Plane Frames Including Changes in Geometry and Nonelastic Behavior of Elements under Combined Normal Force and Bending." **IABSE Symposium on Resistance and Ultimate Deformability of Structures Acted on by Well-Defined Repeated Loads, Lisbon, Portugal.**, Switzerland: 112-123.

Monti, G., and Spacone, E. 2000. "Reinforced Concrete Fiber Beam Element with Bond-Slip." **ASCE Journal of Structural Engineering**. 126, 6: 654-661.

Oehlers, D.J. and Moran, J.P. 1989. "Premature Failure of Externally Plated Reinforced Concrete Beams." **ASCE Journal of Structural Engineering.** 116,4: 978-995.

Rabinovich O., and Frostig Y. 2000. "Closed-Form High-Order Analysis of RC Beams Strengthened with FRP Strips." **ASCE Journal of Composites for Construction.**, 4,2: 65-74.

Roberts, T.M. 1989. "Approximate Analysis of Shear and Normal Stress Concentrations in the Adhesive Layer of Plated RC Beams." **The Structural Engineer**. 67,12: 229-233.

Rubiano-Benavides, N.R. 1998. "Predictions in the Inelastic Seismic Response of Concrete Structures Including Shear Deformations and Anchorage Slip."**Ph.D. Dissertation, Department of Civil Engineering**.University of Texas, Austin,

Saadatmanesh, H., Albrecht, P., and Ayyub, B.M. 1989. "Experimental Study of Prestressed Composite Beams." **ASCE Journal of Structural Engineering**. 115,9: 2349-2364.

Saadatmanesh, H. and Ehsani, M.R. 1991. "RC Beams Strengthening with GFRP Plates. I: Experimental Study." **ASCE Journal of Structural Engineering**. 117,11: 3417-3433.

Spacone, E., Filippou, F.C., and Taucer, F.F. 1996. "Fiber Beam-Column Model for Nonlinear Analysis of R/C Frames. Part I: Formulation." **Earthquake Engineering and Structural Dynamics**. 25: 711-725.

Swamy, R.M., Jones, R., and Bloxham, J.W. 1987. "Structural Behavior of Reinforced Concrete Beams Strengthened by Epoxy-Bonded-Steel Plates." **The Structural Engineer**. 65,2: 59-68.

Täljsten, B. 1997. "Strengthening of Beams by Plate Bonding." **ASCE Journal of Materials in Civil Engineering**. 9,4: 206-212.

Taylor, R.L. 2000. "FEAP: A Finite Element Analysis Program. User manual: Version 7.3" **Department of Civil and Environmental Engineering**.University of California, Berkeley.

Zarnic, R., Gostic, S., Bosiljkov, A., and Bokan- Bosiljkov, V. 1999. "Improvement of Bending Load-Capacity by Externally Bonded Plates." **Proceeding of Creating with Concrete**. London.: 433-442.